

INTEGRATED SEGMENTATION AND DEFORMATION ANALYSIS OF 4-D CARDIAC MR IMAGES

Yun Zhu, Ping Yan, Xenophon Papademetris, Albert J. Sinusas, James S. Duncan

Department of Biomedical Engineering, Department of Diagnostic Radiology
Yale University, New Haven, CT 06520-8042, USA

ABSTRACT

Segmentation and motion estimation from cardiac images are usually considered separately, yet they can obviously benefit from each other. In this paper, we propose a joint segmentation and motion estimation algorithm for the purposes of myocardial deformation analysis and strain estimation. We use segmentation as a guide for selecting feature points with significant shape characteristics, and invoke a Generalized Robust Point Matching (GRPM) strategy with Boundary Element Method (BEM)-based regularization model to estimate the dense displacement field and strain map from 3-D cardiac sequences. Quantitative analysis of the results is performed in comparison with the displacements found using implanted markers, taken to be gold standards.

Index Terms— Cardiac Motion Analysis, Cardiac Image Segmentation, Robust Point Matching, Boundary Element Method

1. INTRODUCTION

Quantitative analysis of left ventricular (LV) deformation at rest and during stress from noninvasive imaging sequences can detect ischemic disease in patients and offer important diagnostic information. There have been a number of efforts in LV deformation analysis [1, 2, 3, 4], of which one important category is to use shape-based tracking algorithm to find the correspondence of the endocardial (ENDO) and epicardial (EPI) borders in two adjacent frames, followed by the dense correspondence interpolation within the myocardium using a biomechanical model. To find the ENDO- and EPI boundaries, Shi used the manual segmentation of the endocardium and epicardium by experts [1]. Lin eliminated the need for manual segmentation by using a Canny edge detector for rough segmentation, followed by the Generalized Robust Point Matching (GRPM) algorithm to find feature point correspondence [2]. Yan extended their work by introducing the Boundary Element Method (BEM) that greatly improves the computational efficiency of the biomechanical model [3].

One of the limitations of these techniques is the lack of an automatic and robust method for segmenting the ENDO-

and EPI boundaries. There has been some limited work on joint LV segmentation and motion estimation. For example, Zhuang proposed a biomechanical model-based method that performs simultaneous LV segmentation and motion estimation [5].

In this paper, we propose an integrated LV segmentation and motion estimation algorithm that uses segmentation as a guide for feature extraction and performs motion estimation directly from intensity images. We do not use segmented boundaries themselves to estimate displacements, thus reducing the dependency on the accuracy of the segmentation. We formulate our approach in a recursive Bayesian framework that segments the myocardium, extracts feature points from the narrowband of segmented contours, and estimates a dense displacement field within myocardium using the BEM-GRPM algorithm [3]. The estimated displacement field is then used to calculate the myocardial strains over multiple frames.

2. GENERAL FRAMEWORK

Let $I_{1:t} = \{I_1, I_2, \dots, I_t\}$ be a collection of images in a cardiac sequence, $S_t = \{S_t^+, S_t^-\}$ be the segmentation at frame t , where S_t^+ is the ENDO surface and S_t^- is the EPI surface. Also, we denote T_t as the transformation function that maps frame $t-1$ to t . The goal is to estimate the state (S_t, T_t) for each frame t , which can be expressed as:

$$\begin{aligned}
 (\hat{S}_t, \hat{T}_t) &= \arg \max_{S_t, T_t} \mathcal{P}(S_t, T_t | I_{1:t}) = \arg \max_{S_t, T_t} \mathcal{P}(S_t, T_t, I_{1:t}) \\
 &= \arg \max_{S_t, T_t} \int \mathcal{P}(S_t, T_t, S_{1:t-1}, T_{1:t-1}, I_{1:t}) dS_{1:t-1} dT_{1:t-1} \\
 &\stackrel{(a)}{=} \arg \max_{S_t, T_t} \int \mathcal{P}(I_t | S_t) \mathcal{P}(S_t | S_{1:t-1}) \mathcal{P}(T_t | S_{t-1}, S_t, I_{t-1}, I_t) \\
 &\quad \mathcal{P}(S_{1:t-1}, T_{1:t-1} | I_{1:t-1}) dS_{1:t-1} dT_{1:t-1} \\
 &\stackrel{(b)}{=} \arg \max_{S_t, T_t} \underbrace{\mathcal{P}(I_t | S_t)}_{\text{data adherence}} \underbrace{\mathcal{P}(S_t | \hat{S}_{1:t-1})}_{\text{shape prior}} \underbrace{\mathcal{P}(T_t | \hat{S}_{t-1}, S_t, I_{t-1}, I_t)}_{\text{shape-based displacements}}
 \end{aligned} \tag{1}$$

This work is supported by 5R01HL082640-02.

where we make three assumptions at step (a) in order to arrive at a computationally more feasible estimation problem:

- T_t is conditioned only on the nearest image frames and their segmentations, i.e. $\mathcal{P}(T_t|S_t, S_{1:t-1}, T_{1:t-1}, I_{1:t}) = \mathcal{P}(T_t|S_t, S_{t-1}, I_{t-1}, I_t)$;
- $I_{1:t}$ are mutually independent, i.e. $\mathcal{P}(I_t|S_t, S_{1:t-1}, T_{1:t-1}, I_{1:t-1}) = \mathcal{P}(I_t|S_t)$;
- Given $S_{1:t-1}$, S_t is conditionally independent of transformations and images in previous frames, i.e. $\mathcal{P}(S_t|S_{1:t-1}, T_{1:t-1}, I_{1:t-1}) = \mathcal{P}(S_t|S_{1:t-1})$.

Also, we assume at (b) that the distributions of previous states to be strongly peaked around the maxima of the respective distributions, i.e. $\mathcal{P}(S_{1:t-1}, T_{1:t-1}|I_{1:t-1}) = \delta(S_{1:t-1} - \hat{S}_{1:t-1}, T_{1:t-1} - \hat{T}_{1:t-1})$, where $(\hat{S}_i, \hat{T}_i) = \arg \max \mathcal{P}(S_i, T_i|I_{1:i})$ are the estimates of the segmentation and deformation obtained in the previous frames, and $\delta(\cdot)$ is the Dirac delta function.

3. DATA ADHERENCE

For each frame t , the entire image is partitioned by S_t^+ and S_t^- into three regions: LV blood pool, LV myocardium, and background. The LV blood pool and myocardium are homogeneous, and therefore can be modeled with a single probability density function (pdf). The most common pdf for MR images is Gaussian distribution which is expressed as

$$P(I_t; \mu_l, \sigma_l) = \frac{1}{\sqrt{2\pi}\sigma_l} \exp\left\{-\frac{(I_t - \mu_l)^2}{2\sigma_l^2}\right\} \quad (2)$$

where μ_l is the mean of Gaussian distribution, and σ_l is its deviation. Equation 2 describes the intensity information for LV blood pool when $l = 1$, and intensity information for LV myocardium when $l = 2$.

The background, however, is inhomogeneous because it contains more than one tissues (RV blood pool, RV myocardium, and lung air). Here, we use a mixture model and invoke EM algorithm to fit the background histogram.

$$\mathcal{P}(I_t; \mu_3, \sigma_3) = \sum_{k=1}^M \alpha_k \mathcal{P}_{3,k}(I_t; \mu_{3,k}, \sigma_{3,k}) \quad (3)$$

where M is the number of components, α_k is the mixture proportion of component k that satisfies $\sum_{k=1}^M \alpha_k = 1$, $\mu_{3,k}$ and $\sigma_{3,k}$ are the mean and deviation of its component distribution. For cardiac MR images, we choose $M = 3$.

Thus, the data adherence term can be defined as follows

$$\log \mathcal{P}(I_t|S_t^+, S_t^-) = \sum_{l=1}^3 \int_{\Omega_{t,l}} \log \mathcal{P}(I_t; \mu_l, \sigma_l) dx \quad (4)$$

where $\Omega_{t,1}$, $\Omega_{t,2}$, and $\Omega_{t,3}$ denote the LV blood pool, LV myocardium, and background respectively. The maximization of equation 4 can be interpreted as the propagation of S_t^+ and S_t^- that maximizes the piecewise homogeneities.

4. INCOMPRESSIBILITY CONSTRAINT

We observe that the volume of myocardium is almost constant during a cardiac cycle [6]. Therefore, we make an assumption that the volume of myocardium at frame t has Gaussian distribution $\mathcal{N}(\bar{V}_t, \sigma_{V_t})$

$$\mathcal{P}(S_t|\hat{S}_{1:t-1}) = \frac{1}{\sqrt{2\pi}\sigma_{V_t}} \exp\left\{-\frac{(V_t - \bar{V}_t)^2}{2\sigma_{V_t}^2}\right\} \quad (5)$$

where $V_t = \int_{\Omega_{t,2}} dx$ is the volume of myocardium enclosed by the ENDO- and EPI surfaces at frame t . Parameter \bar{V}_t and σ_{V_t} can be estimated sequentially using $\bar{V}_t = \frac{1}{t-1} \sum_{i=1}^{t-1} \hat{V}_i$ and $\sigma_{V_t}^2 = \frac{1}{t-1} \sum_{i=1}^{t-1} (\hat{V}_i - \bar{V}_t)^2$.

5. FEATURE EXTRACTION

Our shape-based tracking algorithm requires finding the curvature on the ENDO- and EPI surfaces [1]. While curvature can be computed from segmented surfaces, the curvature operator is a second-order differential operator which amplifies the segmentation errors, and hence requiring very accurate segmentation of the ENDO- and EPI surfaces. An alternative is to compute scaled isophote curvature from intensity images in order to reduce the dependency on the accuracy of segmentation [2]. However, isophote curvature could be unreliable at weak boundaries.

In this paper, we use segmentation to guide the selection of feature points with accurate curvature. In particular, we choose our feature points as follows: 1) For each point on the contour, compute the isophote curvature for all points in its 3×3 neighborhood, and select the curvature maxima whose edge strength $\|\nabla I\|$ is larger than a threshold, called type-1 feature point; 2) If the 3×3 block is noisy without strong edges, use the point on the contour as feature point, called type-2 feature point; 3) Rank all type-1 feature points according to their curvatures in descend order, and discard the lower 1/4 points. In Figure 1, we compare the feature points selected with our approach and Canny edge detector. It can be seen that sparse feature points are selected when using the Canny edge detector, especially at epicardium.

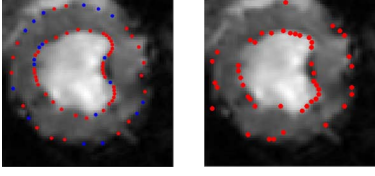


Fig. 1. Comparison of feature points extracted with our approach (left) and Canny edge detector (right). Red: type-1 feature points; Blue: type-2 feature points.

6. SHAPE-BASED DISPLACEMENT ESTIMATION

Assume that $P = \{\mathbf{p}_1, \mathbf{p}_2, \dots, \mathbf{p}_I\}$ and $Q = \{\mathbf{q}_1, \mathbf{q}_2, \dots, \mathbf{q}_J\}$ are two sets of feature points extracted from two adjacent frames. We use BEM-GRPM algorithm to estimate a dense field transformation in a deterministic annealing framework. In particular, we need to maximize the following shape-displacement term:

$$P(T_t | \hat{S}_{t-1}, S_t, I_{t-1}, I_t) \propto \exp\{- (E_{\text{shape}} + \gamma E_{\text{BEM}})\} \quad (6)$$

$$E_{\text{shape}} = \sum_{i=1}^I \sum_{j=1}^J m_{ij} \left(\|T_t \circ \mathbf{p}_i - \mathbf{q}_j\|^2 + \beta_{\kappa} g(\|\kappa(\mathbf{p}_i) - \kappa(\mathbf{q}_j)\|^2) \right) + \tau \sum_{i=1}^I \sum_{j=1}^J m_{ij} \log m_{ij}$$

$$+ \tau_0 \sum_{i=1}^I m_{i,J+1} \log m_{i,J+1} + \tau_0 \sum_{j=1}^{J+1} m_{I+1,j} \log m_{I+1,j}$$

$$E_{\text{BEM}} = \|\mathcal{L} \cdot T_t\|^2$$

where

- β_{κ} is the weight of curvature to proximity information, and is set to zero for type-2 feature points;
- m_{ij} is the correspondence matrix;
- τ is the annealing temperature and τ_0 is the annealing temperature for outliers;
- $\kappa(\mathbf{p}_i)$ is a vector composed of two principal curvatures at \mathbf{p}_i , and $\kappa(\mathbf{q}_j)$ is similarly defined;
- $g(\cdot)$ is a strictly increasing function;
- $\mathcal{L}(\cdot)$ is an operating function on the non-rigid transform T_t . Here, we used BEM-based regularization model for T_t .

7. OPTIMIZATION

The optimization of S_t and T_t from equation 1 can be achieved sequentially by repeating the following two steps:

- **S-step** Fix motion estimation and update segmentation, i.e. $\hat{S}_t = \arg \max_{S_t} \mathcal{P}(I_t | S_t) \mathcal{P}(S_t | \hat{S}_{1:t-1})$. The optimal \hat{S}_t can be identified by the coupled Euler Lagrange equations:

$$\frac{\partial S_t^+}{\partial v} = \left(-\log \left(\frac{\mathcal{P}(I_t; \mu_1, \sigma_1)}{\mathcal{P}(I_t; \mu_2, \sigma_2)} \right) - \frac{V_t - \bar{V}_t}{\sigma_{V_t}^2} \right) \mathbf{n}_t^+$$

$$\frac{\partial S_t^-}{\partial v} = \left(-\log \left(\frac{\mathcal{P}(I_t; \mu_2, \sigma_2)}{\mathcal{P}(I_t; \mu_3, \sigma_3)} \right) + \frac{V_t - \bar{V}_t}{\sigma_{V_t}^2} \right) \mathbf{n}_t^-$$

where v is the time step used to solve the partial differential equations, and \mathbf{n}_t^+ and \mathbf{n}_t^- are the normals of S_t^+ and S_t^- respectively.

- **T-step** Fix segmentation and update motion estimation, i.e. $\hat{T}_t = \arg \max_{T_t} \mathcal{P}(T_t | \hat{S}_{t-1}, S_t, I_{t-1}, I_t)$. The optimal T_t can be obtained using BEM-GRPM algorithm [3].

1. Estimate the correspondence matrix m_{ij} between the point \mathbf{p}_i and \mathbf{q}_j

$$m_{ij} = \frac{1}{\sqrt{2\pi\tau^2}} \exp \left\{ -\frac{1}{\tau} \left(\|T_t \circ \mathbf{p}_i - \mathbf{q}_j\|^2 + \beta_{\kappa} g(\|\kappa(\mathbf{p}_i) - \kappa(\mathbf{q}_j)\|^2) \right) \right\}$$

2. Calculate \mathbf{q}_j 's correspondent point $\hat{\mathbf{q}}_i = \frac{\sum_{j=1}^J m_{ij} \mathbf{q}_j}{\sum_{j=1}^J m_{ij}}$

and the confidence parameters $c_i = \sum_{j=1}^J m_{ij}$;

3. Find the dense transformation T_t by BEM, i.e. $\hat{T}_t = \arg \max_{T_t} \sum_{i=1}^I c_i \|T_t \circ \mathbf{p}_i - \hat{\mathbf{q}}_i\|^2 + \gamma \|\mathcal{L} \cdot T_t\|^2$;

4. If $\tau \geq \tau_{\text{threshold}}$, then $\tau = \tau \cdot \delta$ and go to step 1.

The whole scheme is initialized with the manual segmentation in the first frame, and then use the results from the previous frame to initialize the current frame. Due to similarity to two adjacent frames, it takes around 30 sec to segment one 3-D frame, and 1 min to find the dense correspondence between two 3-D frames.

8. EXPERIMENTS

In this section, we present validation of results on 12 canine MR sequences, which have 16 temporal frames per cardiac cycle [1], with an in-plane resolution of 1.6mm and a slice thickness of 5mm. Figure 2 shows the estimated dense displacement field within myocardium. To further quantitatively evaluate our algorithm, we define the displacement error for point i as $|\mathbf{d}_i - \tilde{\mathbf{d}}_i|$, where \mathbf{d}_i is the estimated displacement and $\tilde{\mathbf{d}}_i$ is the ground truth displacement from the implanted marker [1]. Figure 3 shows the displacement errors during cardiac systole for one cardiac sequence. Table 1 shows the mean and variance of the displacement errors over 12 sequences. It can be seen that while error propagation exists for all three methods, less error is propagated when the segmentation-guided isophote curvature is used. Also, the variance of displacement errors is reduced, which implies the improvement of robustness for motion estimation.

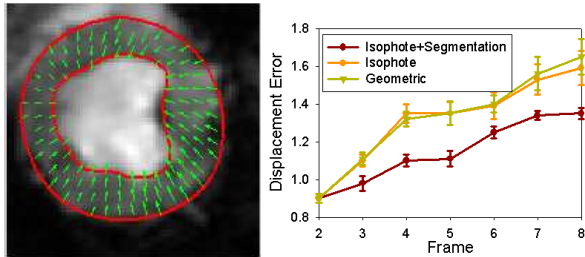


Fig. 2. The short-axis view of the dense displacements derived from tricular systole for one cardiac our approach. **Fig. 3.** Comparison of displacement errors during cardiac sequence.

Table 1. Comparison of displacement errors over 12 cardiac sequences.

	Displacement Error(pixels)
isophote curvature+ segmentation	1.11 ± 0.05
isophote curvature	1.40 ± 0.09
geometric curvature	1.45 ± 0.08

In Figure 4, we show the temporal development of radial and circumferential strains from End-Diastole (ED) to End-Systole (ES) for one 3-D sequence. Note the normal behavior in the left ventricle, showing the positive radial strain (thickening) and negative circumferential strain (shortening) during cardiac systole.

9. CONCLUSION

In this paper, we have presented a joint segmentation and motion estimation algorithm to recover LV deformation. We

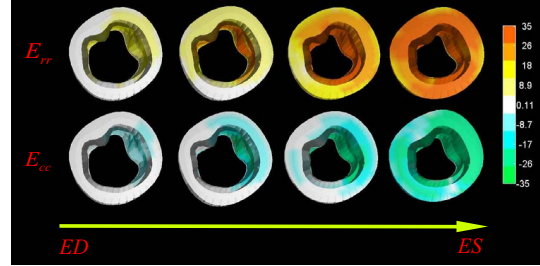


Fig. 4. The development of radial(top) and circumferential(bottom) strains in the left ventricle. The strain patterns are shown at 1/4, 1/2, 3/4, and 4/4 of time between ED and ES.

used coupled ENDO- and EPI segmentation as a guidance to extract robust feature points with significant shape characteristics, and then fed them into BEM-GRPM algorithm to estimate a spatially dense myocardial displacement field and strain map. Future work includes the extension to echocardiographic images where phase-sensitive speckle can be used as a complementary motion information for mid-wall tracking. Also, tissue modeling with more complicated biomechanical models will be considered.

10. REFERENCES

- [1] Pengcheng Shi, Albert J. Sinusas, R. Todd Constable, Erik Ritman, and James S. Duncan, "Point-tracked quantitative analysis of left ventricular surface motion from 3-d image sequences," *IEEE TMI*, vol. 19, no. 1, pp. 36–50, 2000.
- [2] Ning Lin, Xenophon Papademetris, Albert J. Sinusas, and James S. Duncan, "Analysis of left ventricular motion using a general robust point matching algorithm," in *MICCAI*, 2003, pp. 556–563.
- [3] Ping Yan, Albert J. Sinusas, and James S. Duncan, "Boundary element method-based regularization for recovering of lv deformation," *Medical Image Analysis*, vol. 11, no. 6, pp. 540–554, 2007.
- [4] Zhenhua Hu, Dimitris Metaxas, and Leon Axel, "In-vivo strain and stress estimation of the left ventricle from mri images," in *MICCAI*, 2002, pp. 706–713.
- [5] Ling Zhuang, Huafeng Liu, Wei Chen, Hujun Bao, and Pengcheng Shi, "Simultaneous segmentation and motion recovery in 3d cardiac image analysis," in *CVBIA workshop at ICCV*, 2005, pp. 499–507.
- [6] Yun Zhu, Xenophon Papademetris, Albert Sinusas, and James S. Duncan, "Segmentation of myocardial volumes from real-time 3d echocardiography using an incompressibility constraint," in *MICCAI*, 2007, pp. 44–51.